AGU PUBLICATIONS

Geophysical Research Letters

RESEARCH LETTER
10.1002/2015GL067349

Key Points:
- Dissipation and mixing rates on the upper slope are 10 to 100 times more energetic than shelf
- Turbulence is elevated within the bottom 100 m and 10–30 km across the critical latitude
- Locally generated internal tide is trapped along the slope and dissipates its energy

Correspondence to:
I. Fer,
ilker.fer@uib.no

Citation:
Fer, I., E. Darelius, and K. B. Daae (2016), Observations of energetic turbulence on the Weddell Sea continental slope, *Geophys. Res. Lett.*, *43*, doi:10.1002/2015GL067349.

Received 8 DEC 2015
Accepted 4 JAN 2016
Accepted article online 11 JAN 2016

©2016. The Authors.
This is an open access article under the terms of the Creative Commons Attribution-NonCommercial-NoDerivs License, which permits use and distribution in any medium, provided the original work is properly cited, the use is non-commercial and no modifications or adaptations are made.

Observations of energetic turbulence on the Weddell Sea continental slope

Ilker Fer[1], Elin Darelius[1], and Kjersti B. Daae[1]

[1] Geophysical Institute, University of Bergen and Bjerknes Centre for Climate Research, Bergen, Norway

Abstract Turbulence profile measurements made on the upper continental slope and shelf of the southeastern Weddell Sea reveal striking contrasts in dissipation and mixing rates between the two sites. The mean profiles of dissipation rates from the upper slope are 1–2 orders of magnitude greater than the profiles collected over the shelf in the entire water column. The difference increases toward the bottom where the dissipation rate of turbulent kinetic energy and the vertical eddy diffusivity on the slope exceed 10^{-7} W kg^{-1} and 10^{-2} m^2 s^{-1}, respectively. Elevated levels of turbulence on the slope are concentrated within a 100 m thick bottom layer, which is absent on the shelf. The upper slope is characterized by near-critical slopes and is in close proximity to the critical latitude for semidiurnal internal tides. Our observations suggest that the upper continental slope of the southern Weddell Sea is a generation site of semidiurnal internal tide, which is trapped along the slope along the critical latitude, and dissipates its energy in a $\mathcal{O}(100)$ m thick layer near the bottom and within $\mathcal{O}(10)$ km across the slope.

1. Introduction

Mixing processes along the Antarctic continental margins affect the production rates and hydrographic characteristics of descending dense waters contributing to the deep and bottom layers of the Southern Ocean [*Nicholls et al.*, 2009] and the adiabatic upwelling of Antarctic Circumpolar Deep Water [*Mead Silvester et al.*, 2014]. Vertical mixing on the continental slope and shelf of the Weddell Sea is particularly important because this region is a major source of Antarctic Bottom Water [*Orsi et al.*, 1999] and a possible conduit of relatively warm water to the Filchner Ice Shelf (FIS, see Figure 1 for locations) [*Årthun et al.*, 2012; *Darelius et al.*, 2014]. A coarse resolution model suggests a dramatic increase in basal melt rates below FIS caused by increased warm inflow in the future [*Hellmer et al.*, 2012]; however, the uncertainties are large. The extent to which mixing processes affect water mass transformations and exchanges must be adequately represented in numerical models.

The location of the southeastern Weddell Sea continental slope is unique: the critical slope and the critical latitude for the semidiurnal internal tidal waves are colocated [*Robertson*, 2001; *Daae et al.*, 2009]. Here we show that this leads to energetic turbulent mixing on the upper slope, distinct from the quiescent shelf farther south. Internal tides are generated as a result of the tidal flow of stratified water column over topographic variations. A topography with slope s is critical when s is equal to the slope α of an incident internal wave ray. Near-critical bathymetric slopes ($\alpha \sim s$) distort the incident internal wave energy and shear such that the waves are more likely to break and cause mixing [*Eriksen*, 1985; *Nash et al.*, 2004]. A latitude is critical, ϕ_c, when the wave frequency, ω, is equal to the local inertial frequency, f. For the lunar semidiurnal frequency, M_2, ϕ_c is 74°28′. Poleward of ϕ_c, linear waves at the corresponding frequency are evanescent [*Le-Blond and Mysak*, 1978], cannot propagate freely, and dissipate their energy locally. Increased levels of local energy dissipation and turbulent mixing are thus expected.

Tidal dynamics and its internal response near the critical latitude and critical slope lead to energetic currents, increased shear, and mixing rates. On the upper slope at our study site, s varies between 0.5 and 2α [*Daae et al.*, 2009]. Observations on the southern Weddell Sea continental slope [*Foldvik et al.*, 1990] show strongly depth-dependent semidiurnal tidal currents. Using two-dimensional idealized simulations, *Robertson* [2001] shows that the generation of M_2 internal tides in the Weddell Sea is sensitive to the proximity of the shelf break to ϕ_c and the generation is stronger when the continental slope is near ϕ_c. In a three-dimensional regional modeling study of the Weddell Sea, *Pereira et al.* [2002] report an internal tide of moderate strength generated over the slope, which propagates in the alongslope direction and dissipates rapidly. On the continental

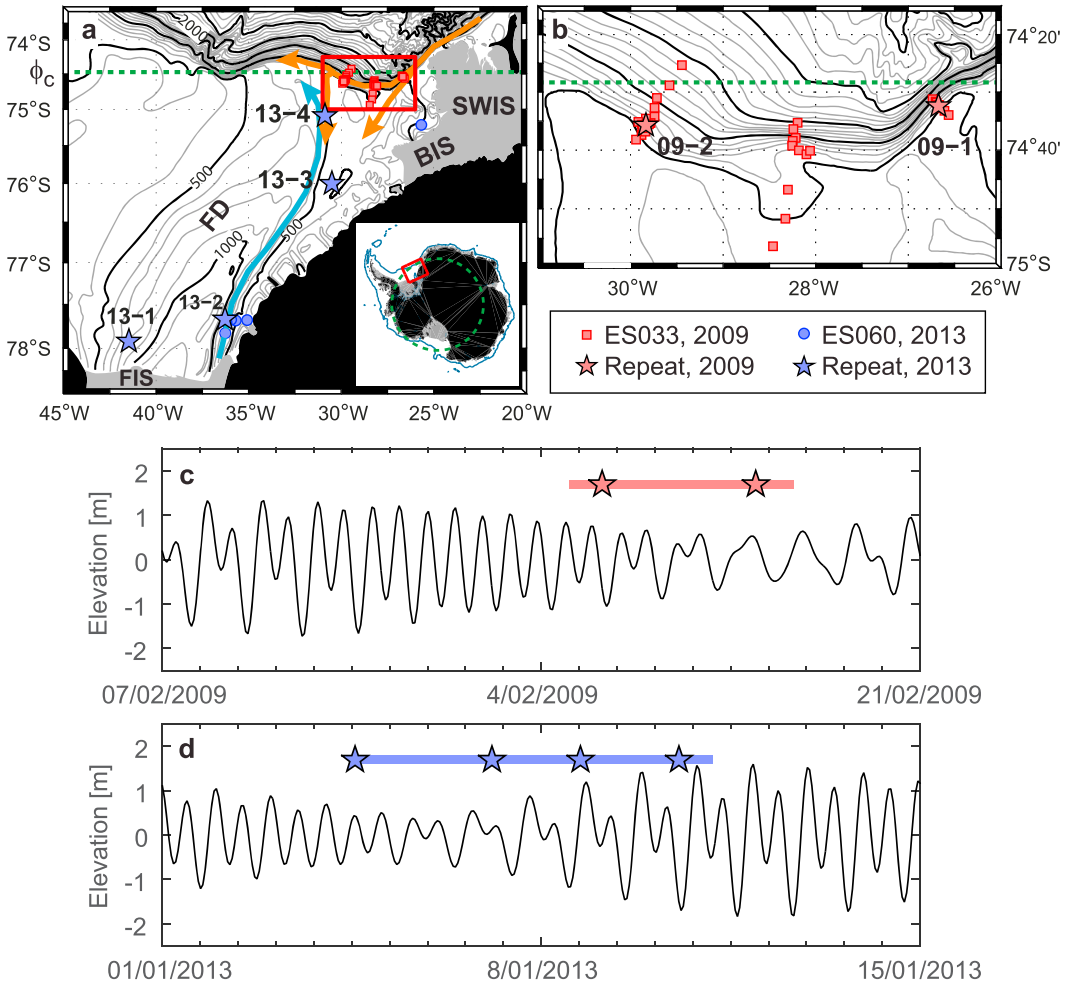

Figure 1. Station map, bathymetry (General Bathymetric Chart of the Oceans), circulation in the region, and the occupation of stations relative to tides. Observations were made in 2009 (red squares) and in 2013 (blue bullets). The stars denote the repeat stations. The red rectangle in Figure 1a is expanded in Figure 1b to show the 2009 stations in detail. The dashed green line marks ϕ_c. The inset in Figure 1a shows the study site together with ϕ_c and the 1000 m isobath. Place names are Filchner Depression (FD), Filchner Ice Shelf (FIS), Brunt Ice Shelf (BIS), and Stancomb-Wills Ice Stream (SWIS). The circulation in the region is shown in Figure 1a by orange (warm inflow) and light blue (cold outflow) arrows [*Nicholls et al.*, 2004; *Darelius et al.*, 2014]. The duration of the measurements and the start of repeat stations are shown together with the CATS tidal elevation at stations (c) 09-2 and (d) 13-2.

shelf and the upper slope, a 150 m thick bottom boundary layer develops near ϕ_c, characterized by high vertical eddy viscosity and diffusivity of up to 10^{-1} m^2 s^{-1}. Limited observations echo this finding: eddy diffusivity inferred from fine-scale parametrization is elevated near the bottom and near the critical latitude [*Daae et al.*, 2009]. These results are further supported by the first direct measurements of microstructure shown here, which contrast the mixing rates at the shelf break of the Weddell Sea and over the shelf in the Filchner Depression (Figure 1a). We show that there are elevated levels of turbulence dissipation concentrated within a 100 m thick layer near the critical latitude, colocated with the upper continental slope. The documented strong spatial variability of turbulent mixing has consequences for the regional heat budget and circulation.

2. Data

Observational data include profiles of temperature, salinity, and horizontal currents using a CTD-LADCP (conductivity, temperature, depth—lowered acoustic Doppler current profiler) system, and microstructure profiles using the vertical microstructure profiler (VMP, Rockland Scientific International). Data were collected during two cruises of the Royal Research Ship Ernest Shackleton: ES033 in February 2009 and ES060 in January 2013. In both cruises a system with dual, pumped CTD (Sea-Bird Electronics, SBE911plus), and dual

ADCPs (300 kHz Sentinel, Teledyne RD Instruments) was used. The VMP system was identical in both cruises. At the stations analyzed here, a CTD-LADCP profile was immediately followed by a VMP cast.

The 2009 stations are concentrated near the continental shelf break and the upper continental slope, along three sections with steep (easternmost section), moderate, and gentle (westernmost section) bottom slopes (Figure 1b). The bottom slope between the 500 m and 1500 m isobaths is 0.03 and 0.17 at the gentle and steep slope sections and are near-critical and supercritical, respectively, for M_2 waves. The steep and gentle slope sections were followed by repeat stations (09-1 and 09-2) of approximately 14 h duration, located near the 600 m isobath and separated by 94 km.

The 2013 data set is from the Filchner Depression. The current and hydrographic observations are described in *Darelius et al.* [2014]. Here we concentrate on stations where current and microstructure sampling occurred: four repeat stations (13-1 to 13-4, each 10–14 h duration) and a section about 30 km from the FIS front.

In total we use 38 profiles collected in 2009 and 34 profiles in 2013. The processing of the CTD-LADCP data is described in *Darelius et al.* [2014]. The processing of the microstructure data follows *Fer et al.* [2012, 2014]. The reduced data set used here consists of profiles of 1 m vertically averaged temperature, T, salinity, S, and potential density anomaly, σ_θ, and 4 m vertically averaged horizontal velocity from the CTD-LADCP system and 2 m vertically averaged dissipation rate, ε, of turbulent kinetic energy from the VMP. Additionally, 1 m vertically averaged T, S, and σ_θ profiles are obtained from the pumped SBE-CTD sensors of the VMP.

The sampling periods are shown relative to tidal forcing in Figures 1c and 1d. The tide data are obtained from CATS [the circum-Antarctic inverse barotropic tidal model, 2008b, an update to *Padman et al.*, 2002]. The environmental conditions (hydrography, currents, wind, sea ice, and tides) were similar in 2009 and 2013, and the observed variability will be interpreted to be spatial (discussed in section 6). For reference, the distance between ϕ_c and 09-01 is 7 km, 09-02 is 14 km, and 13-01 is 396 km.

3. General Features of Currents, Hydrography, and Turbulence

The circulation in the region including the Antarctic slope current, the warm inflow, and the cold outflow is shown in Figure 1a. The slope current is characterized by mean currents of 10–20 cm s^{-1} and subinertial mesoscale variability with similar amplitude that is attributed to trapped vorticity waves [*Jensen et al.*, 2013]. The upper continental slope is thus generally more energetic than the shelf, where the mesoscale variability and the currents are typically weaker, although strong currents (20 cm s^{-1}) were observed in the cold outflow along the eastern flank of the Filchner Depression [*Darelius et al.*, 2014]. Tidal currents, on the other hand, are comparable on the upper slope and on the shelf (the CATS ellipse semimajor axis values at the repeat stations are 6–10 cm s^{-1} for M_2 and 4–6 cm s^{-1} for S_2).

The steep and gentle slope sections collected in 2009 are shown in Figure 2 together with the corresponding 14 h repeat stations near the 600 m isobath. The hydrography is typical of the region with a diffuse pycnocline located at the upper part of the slope separating the cold and less saline surface water from the relatively warm and salty deep water [*Nicholls et al.*, 2009]. A discussion of the currents and stratification measured during the same cruise can be found in *Chavanne et al.* [2010] and *Jensen et al.* [2013].

Snapshots from the two sections show that below the upper turbulent layer directly forced by wind, the dissipation rates are up to 1 order of magnitude elevated over the shelf and decay to the noise level of 10^{-10} W kg^{-1} away from the shelf break. Below the pycnocline, ε increases gradually with depth to 5×10^{-9} W kg^{-1}. A beam of high dissipation rates emanating from bottom at approximately 700 m depth is captured by the outermost three stations of the steep section (Figure 2a), but is absent on the gentle section. Time series from the repeat stations highlight the strong semidiurnal variability. Along- and across-isobath baroclinic currents, (u_a, u_x), are obtained by rotating the velocity vectors (130°, steep section and station 09-1; 240°, gentle section and station 09-2) and then removing the depth average; positive values are toward shallow water and west. The time series are short; however, at the steep section they show a low mode structure (opposing currents in the upper and lower part of the water column). The vertical structure at the gentle section is more complex, affected by higher vertical modes (shorter vertical wavelength). The first mode of baroclinic kinetic energy at the steep station contains 85% of the variance in the first 10 modes, whereas at the gentle slope station only 28% is in the lowest mode (not shown). The negative and positive velocity bands are tilted but with no clear indication on the direction of energy propagation. Phase-locked with the tide, relatively warmer water is recorded in the deepest 100m, which can be attributed to the upslope motion of the pycnocline bringing

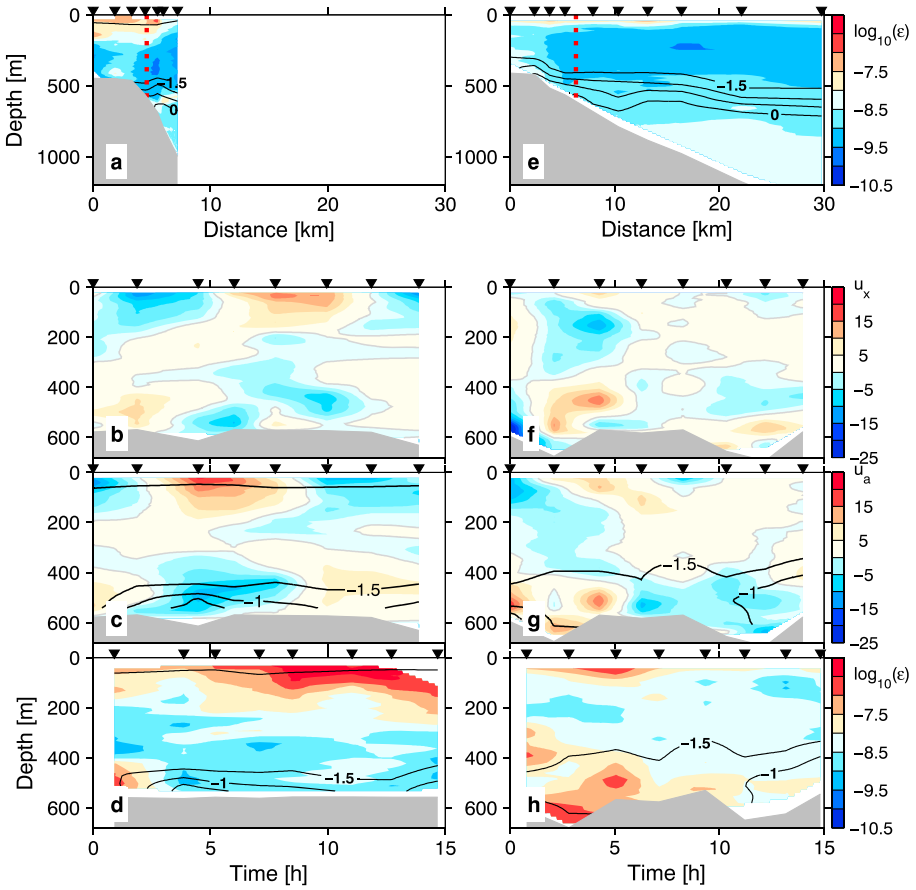

Figure 2. Dissipation rate ε (W kg^{-1}, color) and temperature (black) along the (a) steep and (e) gentle slope sections. The red dashed vertical lines mark the repeat stations (09-1 on steep slope and 09-2 on gentle slope). Data collected at repeat stations (b–d) 09-1 and (f–h) 09-2: (Figures 2b and 2f) cross-isobath and (Figures 2c and 2g) along-isobath baroclinic velocity (cm s^{-1}, color) and temperature (black) measured by CTD-LADCP, and (Figures 2d and 2h) ε (color) and temperature (black) measured by VMP. Bathymetry (gray) is obtained from bottom tracking of the downward pointing ADCP for the CTD-LADCP panels and from the ship's echo sounder for the VMP panels. The topographic variability at repeat stations is due to the ship's movement along the smooth slope.

warmer deep waters to the station. At the repeat stations, ε shows order of one magnitude temporal variability in the bottom 200 m, however, without a clear tidal pattern. The energetic near-bottom turbulence recorded at 09-2 is not captured when the gentle section was worked. The time series at 09-1 is upslope of the turbulent beam at the steep section (see Figure 2a) and, except from the first profile, does not show elevated turbulence levels near the bottom. Stations collected on the shelf in 2013 are characterized by weak dissipation rates ($< 10^{-9}$ W kg^{-1} below 50 m, Figure 3).

4. Bottom-Elevated Turbulence on the Slope

Average profiles of dissipation, ε, and diapycnal eddy diffusivity, K_ρ, are calculated separately for the 2009 and 2013 surveys to contrast the upper slope and the shelf region. An average data point in these profiles is the maximum likelihood estimator of the mean from a lognormal distribution with corresponding 95% confidence intervals. First, average profiles of ε and σ_θ are calculated with respect to depth (isobaric) and height above bottom, separately. The average eddy diffusivity profile is then obtained from $K_\rho = 0.2\varepsilon N^{-2}$ [*Osborn*, 1980], using the buoyancy frequency, $N(z) = \left[-\left(g/\rho_0\right)\partial\sigma_\theta/\partial z\right]^{1/2}$, $\rho_0 = 1028$ kg m^{-3}, and a vertical length scale of 4 m. Segments with weak stratification ($N < 8.7 \times 10^{-4}$ s^{-1}) are excluded from K_ρ.

The comparison between the survey mean profiles of 2009 (upper slope) and 2013 (shelf) is striking (Figure 3). Regardless of averaging with respect to height or depth, the mean profiles from the upper slope are 1–2 orders of magnitude greater than the profiles collected over the shelf. Note that the upper slope stations are

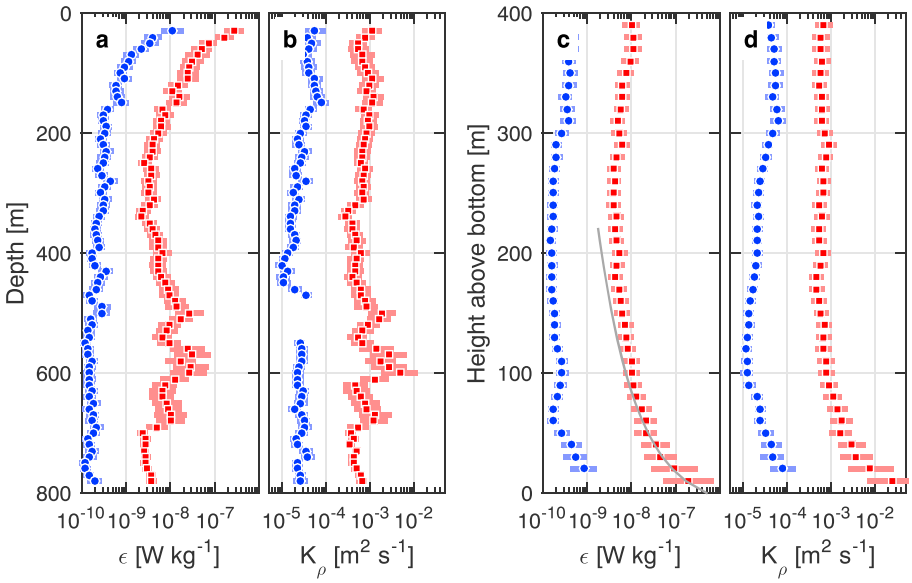

Figure 3. Survey-averaged profiles of (a, c) ε and (b, d) K_ρ averaged with respect to (Figures 3a and 3b) depth and (Figures 3c and 3d) height above bottom. Missing values of K_ρ are segments with weak stratification. The 2009 stations (red squares) are near the shelf break and upper continental slope whereas the 2013 stations (blue bullets) are on the shelf, poleward of ϕ_c. The error bars are the 95% confidence intervals. A curve fit to ε is shown in Figure 3c following *Polzin* [2004].

close to ϕ_c and near the generation site of semidiurnal internal tides [*Daae et al.*, 2009]. Beneath a 100 m thick turbulent upper surface layer, the 2013 mean profiles of ε are close to the noise level of the instrument. At the shelf, K_ρ is of order 10^{-5} m^2 s^{-1}, which is likely an overestimate partly because of weak stratification and also because of not resolving smaller values of ε. When averaged isobarically, the 2009 ε profile is elevated in a 200 m thick layer centered at 600 m depth. This corresponds to the depths of the shelf break, implying increased dissipation and vertical mixing there. When averaged with respect to height from seabed, this layer of energetic turbulence and mixing is limited to the bottom 100 m. Average vertical profiles obtained from the stations over the steep and gentle slope are similar (not shown). Near-bottom mixing rates at the upper continental slope and shelf break of the southern Weddell Sea are highly elevated and decay with height to background values.

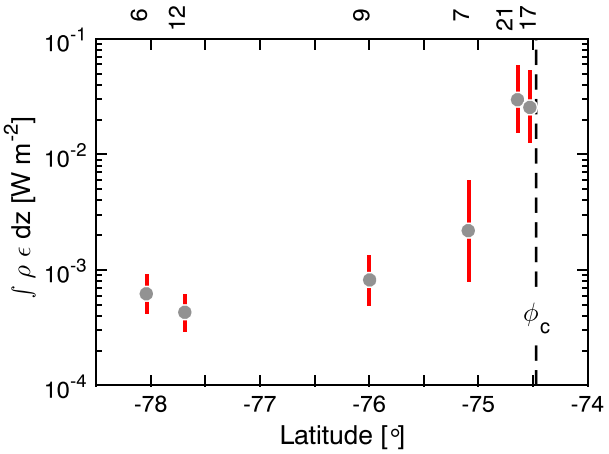

Figure 4. Depth-integrated dissipation rate averaged in latitude bins (0.5° south of 75° and 0.25° north of 75°). The error bars are the 95% confidence intervals. Vertical dashed line marks ϕ_c. The number of profiles averaged in each bin is indicated at top.

5. Elevated Turbulence Near the Critical Latitude

Trapped internal tides are expected to dissipate their energy locally near the generation sites [*Fer et al.*, 2015; *Johnston and Rudnick*, 2014]. The spatial coverage of our stations extends from ϕ_c to approximately 400 km south. Depth-integrated dissipation rate at each station is used to investigate the pattern with respect to distance from ϕ_c. Dissipation averaged in latitude bins is shown in Figure 4. Before integrating in depth, profiles in full water column are obtained by extending the deepest and shallowest measurement to the bottom and surface, respectively (profiling is stopped 5 to 50 m from the

seabed, and the upper 20 m is excluded because of the contamination by the ship's keel). Significant at 95% confidence level, the dissipation gradually peaks toward the critical latitude from the background values on the shelf.

6. Summary and Discussion

Dissipation measurements from two cruises are presented to contrast the mixing rates at the shelf break of the Weddell Sea and farther south, over the shelf and within the Filchner Depression. Energetic turbulence is concentrated within a 100 m thick bottom layer near the critical latitude, colocated with the upper continental slope. Although the cruises are in different years, the data sets are from the similar time of year and under comparable environmental conditions. The difference in vertical structure and magnitudes of dissipation between the two sites is so distinct that it cannot be explained by interannual variability. The tidal forcing is similar in both years (Figures 1c and 1d). A comparison of wind observations (Halley station), wind stress curl (reanalysis products), and sea ice concentration (satellite observations) in 2009 and 2013 shows more energetic and variable winds at Halley in 2013 (twice the mean wind speed and twice the standard deviation compared to 2009), similar regional wind stress and wind stress curl (identical to within one standard deviation), and lower average sea ice concentration over the shelf in 2013 (18% compared to 76% in 2009). The interannual variability would suggest a more energetic water column in 2013, strengthening our interpretations and conclusions on the observed differences between the shelf and upper slope region.

A plausible interpretation of our observations is that the upper continental slope of the southern Weddell Sea generates semidiurnal internal tide, which is trapped along the slope near the critical latitude, and dissipates its energy in $\mathcal{O}(100)$ m thick layer near the bottom and within $\mathcal{O}(10)$ km across the slope. Our study thus confirms and quantifies mixing rates suggested by earlier indirect observations [*Daae et al.*, 2009] and idealized numerical modeling results [*Robertson*, 2001; *Pereira et al.*, 2002].

Elevated dissipation rates near the bottom were previously observed over rough topography [*Polzin et al.*, 1997] or ridges [*Klymak et al.*, 2006]; see *Waterhouse et al.* [2014] for a global scale overview and discussion. In Orkney Passage, boundary mixing caused by coexistence of an internal tide and a downwelling Ekman layer was one of the hypotheses put forward by *Polzin et al.* [2014] to account for the mixing required to close their control volume budget. For a near-bottom wavefield dominated by a baroclinic tide, analytical solutions lead to a dissipation profile as a function of height above bottom, $\varepsilon(z) = \varepsilon_0/(1 + z/z_0)^2$, where ε_0 is the dissipation rate at the bottom and z_0 is decay scale height [*Polzin*, 2004, 2009]. A fit to our average dissipation profile for 2009 (Figure 3c) results in $\varepsilon_0 = 5 \times 10^{-7}$ W kg^{-1} and $z_0 = 14$ m. This is twice the bottom dissipation and one tenth of the decay scale obtained over rough bathymetry in the Brazil Basin [*Polzin*, 2009]. An exponential decay (which would appear linear in the semilog Figure 3c) does not explain our data. The good fit to the analytical form suggests that the increased dissipation rates can be explained by the strongly nonlinear wave-wave interactions. The short decay scale emphasizes the highly nonlinear and, possibly, nonhydrostatic nature of the process. The fit parameters, however, correspond to a vertical scale of 500 m at which the dynamical transitions to, e.g., shear instability should take place. This unrealistically large vertical scale suggests that the closure proposed in *Polzin* [2004] is pushed here beyond dynamical reason.

The distribution of the depth-integrated dissipation with latitude suggests a pattern where the peak near the critical latitude decays poleward (Figure 4). A fit of the form, $a \exp(-y/b)$ where y is the distance referenced to ϕ_c results in an e-folding scale of 17 km. For comparison, this is 9 times the internal Rossby radius.

In addition to the interannual variability, our interpretation has at least two caveats. First, the S_2 constituent is energetic in the region and possible S_2 internal tides are not trapped. Our analysis and presentation of the data do not differentiate between M_2 and S_2, and introduce ambiguity into our interpretation. The M_2 and S_2 ellipse semimajor amplitudes obtained from CATS at the six repeat stations are comparable, but M_2 is 1.5$\pm$0.05 times larger, and we expect its trapped signal to dominate over S_2. Second, the orientation of the tidal ellipses is approximately cross-isobath (stronger internal wave response) at the slope stations and along isobath at the shelf stations. The spatial pattern relative to ϕ_c thus also agrees with the change in relative orientation of tidal velocity and topographic slope. Finally, the slope current and mesoscale activity on the slope can contribute to the observed differences.

The observations presented here show patterns of vertical mixing and energy dissipation with strong vertical and lateral variability, which we attribute to the colocation of critical latitude and critical slope.

Our observations may have relevance for locations where the critical latitude intersects the continental slope in the Amundsen and Ross Seas in Antarctica, and the Chukchi and Beaufort Seas in the Canadian basin of the Arctic Ocean; however, only the Chukchi and Ross Seas have tidal currents comparable to the Weddell Sea. At the site studied here, vertical diffusivities exceed 10^{-2} m^2 s^{-1} near the bottom near the shelf break; the shelf break is the gateway for the deep warm waters on to the shelf and toward the ice shelf cavity and the outflow of cold and dense ice shelf waters (Figure 1a). The observed turbulence patterns may affect the properties of warm inflow onto the shelf and the dense outflow contributing to the bottom waters. Our limited data coverage in the Weddell Sea hinders conclusions on the regional scale. We hypothesize that the study site is a region of strong barotropic to baroclinic tide energy conversion and dissipation, both for diurnal and semidiurnal tides, and the resulting mixing is important for the regional circulation and heat budget. The tidal energetics and signature in mixing in the region merit further studies.

Acknowledgments
This work has been funded by the Research Council of Norway through the NARE program. The data set is available from http://doi.pangaea.de/10.1594/PANGAEA.854379. Constructive comments from two anonymous reviewers and Satoshi Kimura led to a substantially improved manuscript. We thank the crew and the scientists for making the cruises a success. We thank particularly Keith W. Nicholls and Keith Makinson for their help at ES033 and Anna Wåhlin for the loan of the CTD system at ES060.

References

Årthun, M., K. W. Nicholls, K. Makinson, M. A. Fedak, and L. Boehme (2012), Seasonal inflow of warm water onto the southern Weddell Sea continental shelf, Antarctica, *Geophys. Res. Lett.*, *39*, L17601, doi:10.1029/2012GL052856.

Chavanne, C. P., K. J. Heywood, K. W. Nicholls, and I. Fer (2010), Observations of the Antarctic slope undercurrent in the southeastern Weddell Sea, *Geophys. Res. Lett.*, *37*, L13601, doi:10.1029/2010GL043603.

Daae, K. L., I. Fer, and E. P. Abrahamsen (2009), Mixing on the continental slope of the southern Weddell Sea, *J. Geophys. Res.*, *114*, C09018, doi:10.1029/2008JC005259.

Darelius, E., K. Makinson, K. Daae, I. Fer, P. R. Holland, and K. W. Nicholls (2014), Hydrography and circulation in the Filchner Depression, Weddell Sea, Antarctica, *J. Geophys. Res. Oceans*, *119*, 5797–5814, doi:10.1002/2014JC010225.

Eriksen, C. C. (1985), Implications of ocean bottom reflection for internal wave spectra and mixing, *J. Phys. Oceanogr.*, *15*(9), 1145–1156.

Fer, I., K. Makinson, and K. W. Nicholls (2012), Observations of thermohaline convection adjacent to Brunt Ice Shelf, *J. Phys. Oceanogr.*, *42*(3), 502–508, doi:10.1175/jpo-d-11-0211.1.

Fer, I., A. K. Peterson, and J. E. Ullgren (2014), Microstructure measurements from an underwater glider in the turbulent Faroe Bank Channel Overflow, *J. Atmos. Oceanic Technol.*, *31*(5), 1128–1150, doi:10.1175/JTECH-D-13-00221.1.

Fer, I., M. Müller, and A. K. Peterson (2015), Tidal forcing, energetics, and mixing near the Yermak Plateau, *Ocean Sci.*, *11*(2), 287–304, doi:10.5194/os-11-287-2015.

Foldvik, A., J. H. Middleton, and T. D. Foster (1990), The tides of the southern Weddell Sea, *Deep Sea Res., Part A*, *37*(8), 1345–362.

Hellmer, H. H., F. Kauker, R. Timmermann, J. Determann, and J. Rae (2012), Twenty-first-century warming of a large Antarctic ice-shelf cavity by a redirected coastal current, *Nature*, *485*(7397), 225–228, doi:10.1038/Nature11064.

Jensen, M. F., I. Fer, and E. Darelius (2013), Low frequency variability on the continental slope of the southern Weddell Sea, *J. Geophys. Res. Oceans*, *118*, 4256–4272, doi:10.1002/jgrc.20309.

Johnston, T. M. S., and D. L. Rudnick (2014), Trapped diurnal internal tides, propagating semidiurnal internal tides, and mixing estimates in the California Current System from sustained glider observations, 2006 to 2012, *Deep Sea Res., Part II*, *112*, 61–78, doi:10.1016/j.dsr2.2014.03.009.

Klymak, J. M., J. N. Moum, J. D. Nash, E. Kunze, J. B. Girton, G. S. Carter, C. M. Lee, T. B. Sanford, and M. C. Gregg (2006), An estimate of tidal energy lost to turbulence at the Hawaiian Ridge, *J. Phys. Oceanogr.*, *36*(6), 1148–1164.

Le-Blond, P. H., and L. A. Mysak (1978), *Waves in the Ocean*, Elsevier, Amsterdam.

Mead Silvester, J., Y.-D. Lenn, J. A. Polton, T. P. Rippeth, and M. M. Maqueda (2014), Observations of a diapycnal shortcut to adiabatic upwelling of Antarctic Circumpolar Deep Water, *Geophys. Res. Lett.*, *41*, 7950–7956, doi:10.1002/2014GL061538.

Nash, J. D., E. Kunze, J. M. Toole, and R. W. Schmitt (2004), Internal tide reflection and turbulent mixing on the continental slope, *J. Phys. Oceanogr.*, *34*(5), 1117–1134.

Nicholls, K. W., K. Makinson, and S. Østerhus (2004), Circulation and water masses beneath the northern Ronne Ice Shelf, Antarctica, *J. Geophys. Res.*, *109*, C12017, doi:10.1029/2004JC002302.

Nicholls, K. W., S. Østerhus, K. Makinson, T. Gammelsrød, and E. Fahrbach (2009), Ice-ocean processes over the continental shelf of the southern Weddell Sea, Antarctica: A review, *Rev. Geophys.*, *47*, RG3003, doi:10.1029/2007RG000250.

Orsi, A. H., G. C. Johnson, and J. L. Bullister (1999), Circulation, mixing, and production of Antarctic Bottom Water, *Prog. Oceanogr.*, *43*(1), 55–109.

Osborn, T. R. (1980), Estimates of the local rate of vertical diffusion from dissipation measurements, *J. Phys. Oceanogr.*, *10*(1), 83–89.

Padman, L., A. Fricker, R. Coleman, S. Howard, and S. Erofeeva (2002), A new tidal model for the Antarctic ice shelves and seas, *Ann. Glaciol.*, *34*, 247–254, doi:10.3189/172756402781817752.

Pereira, A. F., A. Beckmann, and H. H. Hellmer (2002), Tidal mixing in the southern Weddell Sea: Results from a three-dimensional model, *J. Phys. Oceanogr.*, *32*(7), 2151–2170.

Polzin, K. L. (2004), Idealized solutions for the energy balance of the finescale internal wave field, *J. Phys. Oceanogr.*, *34*, 231–246.

Polzin, K. L. (2009), An abyssal recipe, *Ocean Modell.*, *30*(4), 298–309, doi:10.1016/j.ocemod.2009.07.006.

Polzin, K. L., J. M. Toole, J. R. Ledwell, and R. W. Schmitt (1997), Spatial variability of turbulent mixing in the abyssal ocean, *Science*, *276*, 93–96.

Polzin, K. L., A. C. Naveira Garabato, E. P. Abrahamsen, L. Jullion, and M. P. Meredith (2014), Boundary mixing in Orkney Passage outflow, *J. Geophys. Res. Oceans*, *119*, 8627–8645, doi:10.1002/2014JC010099.

Robertson, R. (2001), Internal tides and baroclinicity in the Southern Weddell Sea 2. Effects of the critical latitude and stratification, *J. Geophys. Res.*, *106*(C11), 27,017–27,034.

Waterhouse, A. F., et al. (2014), Global patterns of diapycnal mixing from measurements of the turbulent dissipation rate, *J. Phys. Oceanogr.*, *44*, 1854–1872, doi:10.1175/JPO-D-13-0104.1.